JOURNAL OF GEOPHYSICAL RESEARCH, VOL. 113, C08017, doi:10.1029/2007JC004540, 2008

Radiometric measurements of ocean surface thermal variability

Chelle L. Gentemann[1,2] and Peter J. Minnett[2]

Received 4 September 2007; revised 28 February 2008; accepted 26 March 2008; published 8 August 2008.

[1] Measurements of diurnal temperature variability at the ocean surface have been available primarily from satellite Sea Surface Temperature (SST) retrievals and a small number of ship-based radiometers. Since most areas are sampled from polar orbiting satellites at most twice a day, surface diurnal variability studies relied on theoretical modeling or extrapolation of results from in situ measurements at depth. The ocean surface responds very rapidly to changes in fluxes of heat and momentum, therefore diurnal variability at the ocean surface may be quite different than heating at depth. Measurements from the Marine Atmospheric Emitted Radiance Interferometer (M-AERI) provide one of the few skin SST data sets augmented by ancillary measurements necessary for investigations into surface diurnal heating and cooling. This unique data set spans all major ocean basins and contains many days with diurnal warming. The timing of the peak in diurnal warming is directly related to the minimum wind speed and varies from 8:00 to 18:00 local-mean-time. Fluctuations in wind speed can result in multiple peaks in diurnal heating during a single afternoon. As wind speed increases, diurnal warming decreases (negatively correlated) and as insolation increases, diurnal warming increases (positively correlated). Changes in wind speed affect diurnal warming amplitudes very rapidly, while changes in insolation have a more gradual effect. The maximum correlation of wind speed (insolation) with changes in diurnal warming is at a time lag of 0 (50) min.

Citation: Gentemann, C. L., and P. J. Minnett (2008), Radiometric measurements of ocean surface thermal variability, *J. Geophys. Res.*, *113*, C08017, doi:10.1029/2007JC004540.

1. Introduction

[2] During the day, the upper ocean is heated by solar radiation. At the air-sea interface there normally exists a heat flux from the ocean to the atmosphere which creates a thin thermally stratified layer. Within this thin viscous layer, commonly referred to as the cool skin layer, molecular forces dominate and molecular conduction is the primary mechanism for heat transfer. As shown in Figure 1, this skin-layer "rides" on top of any warming or cooling within the upper ocean and is responsible for a small difference (0.1 to 0.3 K) between the skin and subskin Sea Surface Temperatures (SST_{skin} and $SST_{subskin}$). Below the skin, the upper ocean layer is known as the "mixed layer" because turbulence often results in a well-mixed layer with little stratification (Figure 1a). Yet, mixed-layer is often a misnomer as stratification may be introduced either by solar warming or precipitation, creating vertical temperature and density gradients (Figure 1b). Within the mixed layer, thermal stratification established by solar heating is referred to as a diurnal warm layer or diurnal thermocline. Vertical temperature gradients within the diurnal thermocline result from the absorption of radiation at differing depths (determined by the absorptivity of the water), vertical diffusion of heat, vertical stratification, and the rate of turbulent mixing within the mixed layer. The temperature profile in the upper ocean, $T(z)$, may be defined as the summation of the bulk or mixed-layer temperature, T_{depth}, diurnal warming, $\Delta T_{dw}(z)$, and cool skin, $\Delta T_c(z)$:

$$T(z) = \Delta T_c(z) + \Delta T_{dw}(z) + T_{depth}. \quad (1)$$

[3] The temperature at the air-sea interface, $T(0)$, is well approximated by SST_{skin}, and may then be written as the diurnal warming at the surface, $\Delta T_{dw}(0)$, or ΔT_{dw}, and the cool skin effect at the surface, $\Delta T_c(0)$, or ΔT_c:

$$SST_{skin} = \Delta T_c + \Delta T_{dw} + T_{depth}. \quad (2)$$

[4] The cool skin is present both day and night. As the oceanic heat loss exceeds heat gained, the surface layer cools and, if present, the diurnal warming diminishes. The cooler, denser water near the surface is gravitationally unstable and results in free convection, overturning the mixed layer and causing temperature gradients to diminish. Stratification also may be decreased by surface wind stress-induced mechanical mixing of the upper ocean, by shear-flow instabilities, or by breaking internal waves.

[5] Increased daytime stratification due to diurnal warming was first recognized in 1942 [*Sverdrup et al.*, 1942] and has been studied extensively since [*Defant*, 1961; *Donlon et al.*, 2002; *Fairall et al.*, 1996; *Schluessel et al.*, 1990;

[1]Remote Sensing Systems, Santa Rosa, California, USA.
[2]Rosenstiel School of Marine and Atmospheric Science, University of Miami, Miami, Florida, USA.

0148-0227/08/2007JC004540$09.00

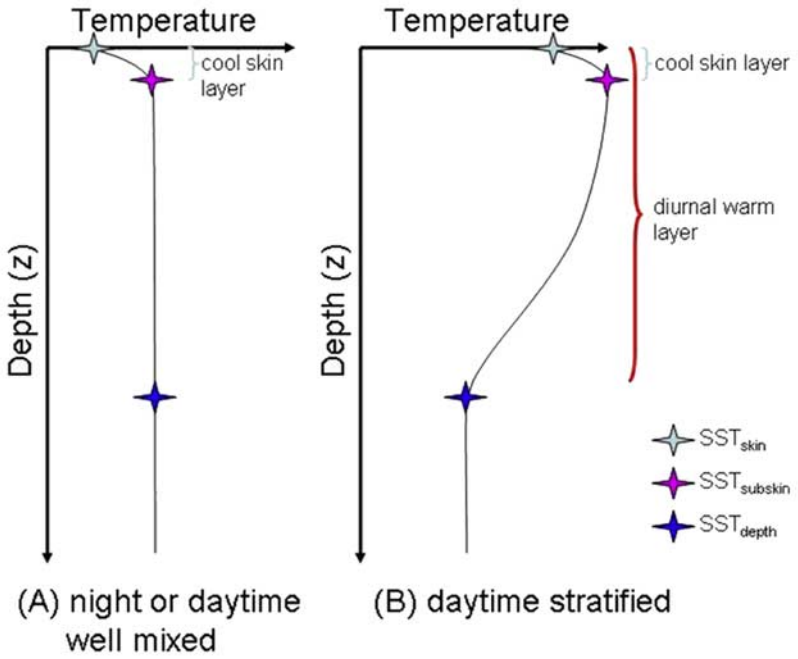

Figure 1. Schematic showing the upper ocean temperature profiles during the (A) nighttime or well mixed daytime and (B) daytime during conditions conducive to the formation of a diurnal warm layer.

Woods and Barkmann, 1986]. Surface temperature deviations greater than 3.0 K, referenced to subsurface temperatures below the extent of surface heating, are not uncommon and may persist for hours [*Kawai and Wada*, 2007; *Minnett*, 2003; *Yokoyama et al.*, 1995]. Even larger amplitudes of diurnal warming (up to 4–6 K) have been reported in several studies [*Flament et al.*, 1994; *Merchant et al.*, 2008; *Stramma et al.*, 1986; *Ward*, 2006]. Failing to account for a diurnal cycle in (SSTs) leads to errors in determining surface fluxes for numerical weather prediction (NWP) and climate models [*Webster et al.*, 1996; *Woods et al.*, 1984]. Tropical atmospheric circulation is sensitive to relatively small changes in SSTs [*Palmer and Mansfield*, 1984; *Shukla*, 1998] as is local atmospheric convection [*Chen and Houze*, 1997] and SST variability in this region is important to understanding climate change.

[6] There is increasing interest in including satellite-based retrievals of SSTs in the historical record for climate applications. Satellite data can provide much needed measurements in remote or data-sparse regions and often lead to a more realistic representation of the spatial and temporal structure of seasonal and interannual variability and an improved reconstruction of global SST. NWP, climate, and mesoscale oceanography require remotely sensed SSTs with an accuracy of 0.1–0.3 K [*GOOS Implementation Advisory Group* (*IAG*), 1999]. Since diurnal warming of the ocean surface can reach amplitudes of 3.0 K or more, an improved understanding of diurnal warming is necessary to meet these temperature accuracy requirements. Blending SST retrievals made at different depths and different times of the day also requires a model of diurnal variability [*Donlon et al.*, 2007]. Additionally, since diurnal warming affects the temperature of the ocean surface which is in direct contact with the atmosphere, improved estimates of diurnal warming will lead to better estimates of air-sea heat and gas fluxes.

2. Background

[7] *Stommel* [1969] and *Stommel and Woodcock* [1951] took some of the earliest measurements of diurnal warming in the ocean. Profiles of upper ocean temperature were taken with a bathythermograph in the Gulf of Mexico, in April 1942, revealing wave-like variations in the upper ocean heat content. In March 1968, the R/V *Chain* deployed a number of Salinity-Temperature-Depth (STD) profilers with the goal of examining diurnal warming. The cruise took place in the southwest North Atlantic Ocean. Insolation was measured with an Eppley Laboratory pyrheliometer. By 9:30 Local-Mean-Time (LMT), a diurnal warm layer was observed; it continued to grow to 0.9 K by 14:15 LMT and then began to decay. The depth of the diurnally heated layer extended to 12 m. Stommel reported classical cooling from the surface where isotherms relaxed toward vertical and the warm layer deepened until all evidence of the warm layer was erased. Using the 1-D heat equation, he was able to roughly balance the radiative forcing with observed heating in the warm layer. Several other early measurements of diurnal warming were also focused on calculating the heat content [*Delnore*, 1972; *Halpern and Reed*, 1976; *Kaiser*, 1978].

[8] Measurements have shown that the vertical profile of diurnal warming in the upper ocean is highly variable [*Minnett and Ward*, 2000; *Ward*, 2006] and therefore models developed from in situ measurements at depth may not fully describe the variability at the ocean surface skin layer. The validity of both the theoretical and empirical models in the skin layer has been explored by a limited

number of studies. In the past, measurements of diurnal temperature variability in the ocean skin layer have been primarily available only from satellite SST retrievals and a few skin radiometers deployed on oceanographic cruises.

[9] The launch of the Heat Capacity Mapping Radiometer (HCMR) in April 1978 prompted the first study relating diurnal warming to wind speed using satellite data in the Mediterranean [*Deschamps and Frouin*, 1984]. The HCMR had two channels at 0.5–1.1 μm and at 10.5–12.5 μm. The satellite was in a sun-synchronous orbit with a Local Equatorial Crossing Time (LECT) of 2:00 AM/PM, close to the average time of the peak of diurnal warming in the ocean. The visible channel was useful for detecting surface sun glitter patterns which are related to wind speed and the infrared channel was used to estimating SST. *Deschamps and Frouin* [1984] reported observing a maximum warming of 5 K, larger than any previous studies. This is likely due to the larger region they were able to examine using the satellite data. These large warming events led them to suggest that when using SSTs to estimate heat content, it would be better to either use only nighttime data or restrict day-time data to winds greater than 5 ms^{-1} to minimize the influence of diurnal warming.

[10] More recently, *Gentemann et al.* [2003] used seventeen years of satellite SST measurements to examine diurnal warming at the ocean surface. SST measurements from the Advanced Very High Resolution Radiometer (AVHRR) carried on several NOAA satellites and the Tropical Rainfall Measuring Mission (TRMM) Microwave Imager (TMI) [*Kummerow et al.*, 1998; *Wentz et al.*, 2000] were collocated with daily average wind speeds from the Special Sensing Microwave Imager (SSM/I) [*Wentz*, 1997]. These data were used to examine how observed diurnal warming at the ocean surface depended on wind speed and insolation. The TRMM satellite LECT drifts through the diurnal cycle every 23 d, providing measurements throughout the diurnal cycle. Since most polar orbiting satellite measurements revisit the same location infrequently, it is only possible to determine the statistical characteristics of diurnal warming. The model developed by *Gentemann et al.* [2003] determined the average diurnal variability throughout the day, as a function of instantaneous wind speed and local time. The local time was utilized to calculate Top-Of-Atmosphere (TOA) clear sky insolation. This model successfully simulated the average diurnal variability throughout the day but did not consider any integrated effect of wind induced mixing or radiative changes due to cloud cover.

[11] Using data from two research cruises, *Minnett* [2003] examined diurnal warming represented by the difference between SST_{skin}, measured by the Marine-Atmospheric Emitted Radiance Interferometer (M-AERI) [*Minnett et al.*, 2001], minus SST_{depth}, the subsurface bulk temperature measured by a thermosalinograph (TSG) at 3 m. Differences as large as 4 K were present at low wind speeds and attributed to diurnal warming. Warming was present at wind speeds up to 5 to 6 ms^{-1}. Since the skin is usually cooler than the bulk, these positive differences between the depth of the bulk thermometer and the skin layer were attributed to diurnal warming.

[12] Another ship-based study of diurnal variability at the skin layer and depth was completed by Jessup and Branch [*Jessup and Branch*, 2008]. Observations of the ocean skin temperature from the Calibrated InfraRed In situ Measurement System (CIRIMS) [*Jessup and Branch*, 2008], the temperature at both 2 m and 3 m depth from through-the-hull port measurements, and the temperature at 5 m depth from the ship's TSG were collected on the R/V *Thompson*. Measurements from 3 to 5 March 2004 show three days with distinct diurnal warming. During the first two days, the diurnal warming at the skin, 2 m, and 3 m measurements are very similar while the 5 m had little to no warming. On the third day, the wind speed was very low and the warming observed is dependent on depth. The skin and 2 m measurements are similar and show roughly 1 K warming, while the 3 m measurements show less warming (only about 0.5 K) and the 5 m measurements show no warming. Although the three days studied do not show any difference between the skin and 2 m measurements of diurnal variability, it is likely that there are differences at lower wind speeds as the diurnal thermocline thickness decreases due to decreased mechanical mixing in the upper ocean.

[13] The study reported here utilizes a large data set of diurnal variability measured at the ocean surface by the M-AERI. The objective of this research is to develop a description of the temporal variability of diurnal warming at the ocean surface using measurements of the skin temperature, a cool skin model, and measurements of the bulk temperature. The studies described above detail the differences between warming measured at different depths. Understanding the diurnal variability at the air-sea interface should improve the understanding of diurnal cycles in air-sea heat and gas fluxes as related to changes in ocean temperature at the air-sea interface and lend guidance for diurnal models used to correct satellite SST_{skin} and $SST_{subskin}$ measurements to a "foundation temperature" [*Donlon et al.*, 2001].

3. Data

[14] The M-AERI is a sea-going modified AERI. The AERI was originally developed for the Department of Energy Atmospheric Radiation Measurement (ARM) program [*Knuteson et al.*, 2004a, 2004b]. The instrument detectors receive radiation, in the form of time varying interferograms, reflected by a scan mirror which views sky, sea-surface, and internal calibration reference blackbodies which are traceable to National Institute of Standards and Technology (NIST) standards [*Rice et al.*, 2003]. A full sequence is completed about every 10 min, fixing the temporal sampling of the instrument. The M-AERI is a Fourier-transform interferometer that measures radiation at 3 to 18 μm wavelengths. SST is retrieved using sea and sky view data at 7.7 μm [*Minnett et al.*, 2001]. The instrument enters a safe mode during rain to avoid contamination of the scan mirror and has been installed temporarily on a number of research vessel and permanently on a cruise ship. The cruises used in this study are depicted in Figure 2. All data were quality controlled and erroneous data were removed from further analysis [*Gentemann*, 2007]. Furthermore, wind and radiation measurements were averaged to 1-min values and then colocated in time, with M-AERI measurements at the midtime of the sea-view measurements. All

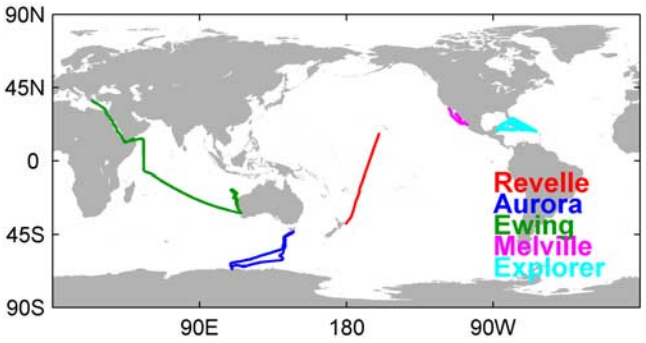

Figure 2. All cruises used in this research.

wind speed measurements were converted to true wind speed and then to a 10 m wind speed using a logarithmic profile. A logarithmic profile rather than an equivalent neutral stability wind was utilized because the differences between the two adjustments are relatively small [*Mears et al.*, 2001]. As with earlier studies [*Donlon et al.*, 2002], there is no attempt here to correct for the ship's effect on measured wind velocity. A discussion of each cruise data set (data measured, instrument specifications is presented in the next section and further details in the Appendix A).

3.1. The *Explorer of the Seas*

[15] A partnership between Royal Caribbean International and the University of Miami's Rosenstiel School of Marine and Atmospheric Science has resulted in placement of oceanographic and atmospheric instrumentation onboard the cruise ship *Explorer of the Seas* [*Williams et al.*, 2006]. The *Explorer of the Seas* is a Voyager-class cruise ship (311 m long, 48 m wide, and 15 decks high) capable of cruising at 12 ms^{-1}. The ship was built with laboratory space and extensive oceanographic and meteorological instrumentation (Table 1). The ship's cruise tracks are shown in Figure 3. During each weekly cruise, the ship makes two long daytime passages to and from its main destination and these segments represent the majority of daytime data used in this study.

[16] The M-AERI was mounted on the starboard side of the *Explorer of the Seas,* measuring SST_{skin} ahead of the bow wake, and has been providing data since 2000. Bulk SST was measured by a TSG located in the bow thruster seawater intake also on the starboard side of the ship, slightly forward from the M-AERI, at a depth of 2 m. Wind speed and direction, corrected for ship motion, were available from three R.M. Young anemometers on the ship, one located at the bow and two located on the port and starboard yardarms of the main mast. Bow wind speed was measured at 24 m above the waterline while the port and starboard winds were at 45 m. The roof of the atmospheric laboratory is instrumented with Eppley radiometers to measure incident shortwave radiation.

3.2. R/V *Aurora Australis*

[17] The M-AERI was deployed on the Australian research ice breaker R/V *Aurora Australis* from 11 September through 29 October 2003, in which time, the vessel departed Hobart, Tasmania for the pack ice near Casey Station on the Antarctica coast, and returned to Hobart. This cruise provides a unique high wind, low insolation polar validation data set. The ship was also instrumented to measure a number of meteorological variables. Wind speed was measured by R.M. Young wind anemometers located on both the Port and Starboard sides of the ship at heights of 31.6 m. Bulk SSTs were acquired by a SeaBird SBE21 TSG installed in the oceanographic laboratory, with an intake at 7 m depth.

3.3. R/V *Ewing*

[18] From 4 August through 30 November 2001, the R/V *Ewing* cruised from Piraeus, Greece, through the Suez Canal, to Fremantle, Australia, with M-AERI installed on the port side, measuring SST forward of the ship's bow wave. Meteorological variables were also acquired from a weatherpak mounted to the main-mast platform at a height of 12 m. Bulk SSTs were acquired from the ship's SeaBird SBE21 TSG with an intake at 4 m depth.

3.4. R/V *Melville*

[19] The M-AERI was onboard the Scripps Institution of Oceanography (SIO) R/V *Melville* for the Marine Optical Characterization Experiment-5 (MOCE-5) program that occurred 1–21 October 1999. The ship left San Diego for the Gulf of California, staying briefly off of the west coast of Mexico. Meteorological data were also collected during the cruise from the ship's forward mast by a R.M. Young

Table 1. List of Instruments and Parameters on the *Explorer of the Seas*[a]

Manufacturer	Instrument	Height	Parameters	Units	Uncertainty
Space Science and Engineering Center, University of Wisconsin-Madison	M-AERI	33 m	skin temperature	K	<0.1[b]
Coastal Environmental Systems, Inc.	wind vane 5103	24 m	wind speed	ms^{-1}	0.3[c]
			wind direction	°	3.0[2]
RM Young	wind vane 1057	45 m	wind speed	ms^{-1}	0.3[d]
			wind direction	°	3.0[3]
Eppley Laboratory	total ultraviolet radiometer (PUV)		ultraviolet radiation	Wm^{-2}	3.5%
	precision infrared radiometer (PIR)		long wave radiation	Wm^{-2}	<5%[e]
	precision spectral pyranometer (PSP)		short wave radiation	Wm^{-2}	1%
SeaBird	21 thermosalinograph		bulk temperature	°C	0.01

[a]Units are given in original file format.
[b]*Minnett et al.* [2001].
[c]Coastal Environmental Systems, Inc., Wind Monitor 5103 brochure.
[d]R.M. Young, Inc. Wind vane 1057 brochure.
[e]http://aadc-maps.aad.gov.au/metadata/mar_sci/Dz200203020.html.

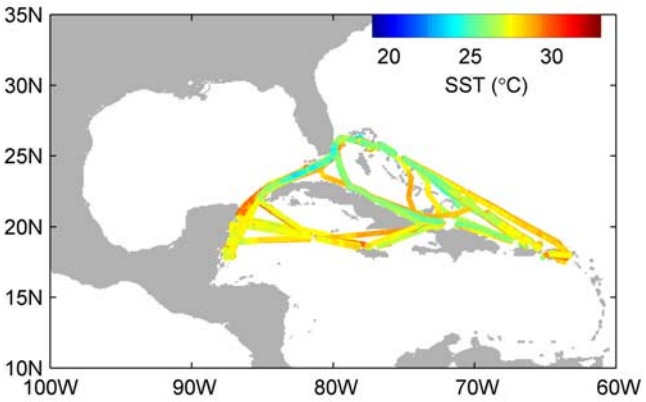

Figure 3. M-AERI SST along cruise tracks for the Explorer of the Seas. Data taken when the ship was in port were not usable, and the diurnal warming analyzed here were from the two days each week that the ship travels to and from Miami on the longer legs. The measured SST_{skin} is indicated by color.

anemometer and Eppley radiometers. Wind measurements were taken at a height of approximately 19 m. Bulk temperature was taken by a Seabird SBD-45 TSG at a depth of 3 m. The M-AERI retrieved air temperature and SST_{skin} approximately every 11 min from 1–21 October 1999.

3.5. R/V *Revelle*

[20] The R/V *Revelle* left Honolulu, HI on 25 September 1997, arriving into Lyttleton, NZ on 14 October 1997. Two M-AERIs were installed side-by-side and examined for consistency. The two M-AERIs measured SST_{skin} to within 0.1 K of each other [*Minnett et al.*, 2001]. An Alden Improved METeorological (IMET) system that provides wind speed, wind direction, relative humidity, barometric pressure, long and shortwave radiation, air temperature, sea surface temperature, and precipitation [*Hosom et al.*, 1995] was located at the bow of the ship, on a science mast. The ship's anemometers are located on the main mast, above the pilot house. The height of the anemometers was estimated by the Data Assembly Center (DAC) to be 22 m. Bulk sea surface temperatures and salinities are reported from Falmouth Scientific Inc. (FSI) temperature/conductivity sensors. One pair of measurements is from the bow thruster room where water is fed by ship motion. From the ship's schematic, this is estimated to be at a depth of 3 m.

[21] The data used here are from a single M-AERI that retrieved air temperature and SST_{skin} approximately every 18 min from 30 September through 3 October 1997. From 4–6 October the M-AERI recorded approximately every 14 min, on 7 October the M-AERI recorded data approximately every 7 min, from 8–12 October every 10 min, and on 13 October data were recorded every 8 min.

3.6. Calculation of Diurnal Variability

[22] As shown in (2), the temperatures observed by M-AERI at the ocean surface are a summation of the bulk mixed layer temperature, a diurnal thermocline, and the cool skin layer. Therefore the diurnal warming at the surface is:

$$\Delta T_{dw} = SST_{skin} - \Delta T_c + SST_{depth}, \tag{3}$$

where SST_{skin} is measured by M-AERI, ΔT_c may be estimated using a simple model, and T_{depth}, is measured at depth by a TSG installed onboard the various ships. Figure 4 shows the difference, SST_{skin} minus SST_{depth}, as a function of wind speed along with a least squares fit to the M-AERI data using an exponential equation formulation, the *Donlon et al.* [2002] cool skin layer estimate (hereafter D2002), and the mean value at each 1 ms^{-1} wind speed interval. These data are from the *Explorer of the Seas* cruises, excluding data between 6 November 2002 to 27 January 2003 and 30 June 2004 to 2 November 2005. The least squares fit to the *Explorer of the Seas* data shows remarkably close agreement to the D2002 parameterization. Therefore the D2002 cool skin estimate was subtracted from the M-AERI SST_{skin} in this study to estimate $SST_{subskin}$. This correction was applied to all data. The D2002 parameterization was chosen for several reasons. A newer parameterization from *Horrocks et al.* [2003] uses the same exponential parameterization but finds slightly different coefficients. D2002 is based on a larger data set and we therefore chose this over the Horrocks parameterization. Both papers note that there is increased uncertainty below 2 ms^{-1}. Although these cool skin parameterizations were developed using only nighttime data, they also provide an accurate representation of the daytime cool skin effect, as discussed by Minnett et al. (P. J. Minnett et al., Measurements of the oceanic thermal skin effect, submitted to *Deep-Sea Research II*, 2008) who found a similar dependence on wind speed.

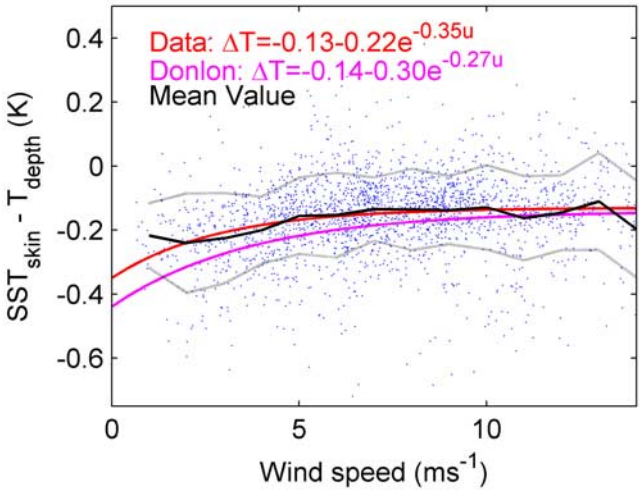

Figure 4. Nighttime difference, M-AERI SST_{skin} minus TSG SST_{depth}, as a function of wind speed. The least squares fit to the data is shown in red, the mean and standard deviation of the data, calculated at 1 ms^{-1} intervals, are respectively shown by the black solid and dotted lines.

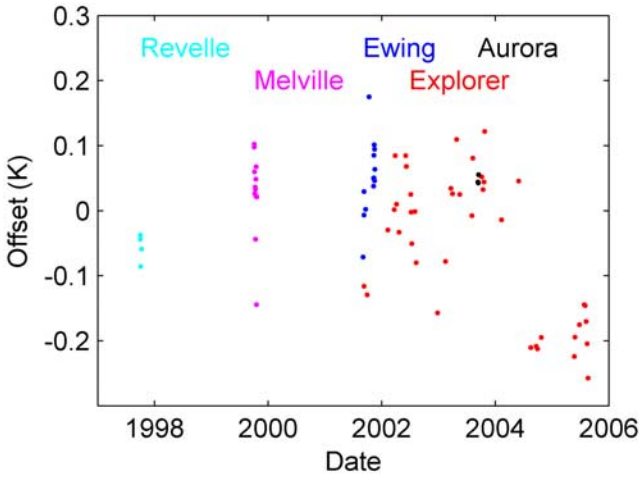

Figure 5. Daily offsets subtracted from M-AERI skin minus TSG bulk temperatures to normalize the daily diurnal warming amplitudes.

[23] A secondary correction to the data was needed to account for small differences between the M-AERI SST_{skin} minus the modeled cool skin and SST_{depth}. In this data set, no significant diurnal warming persisted from one day into the next. Therefore $SST_{subskin}$ and SST_{depth} should be equivalent prior to daytime diurnal warming and ΔT_{dw} equal to zero. On some days within individual cruises this relationship held true, but occasionally there remained a small offset, usually less than 0.1 K (Figure 5). These differences may be due to seasonal heating and cooling, spatial gradients in the mixed layer temperature gradients, low levels of fouling in the intake, TSG calibration errors, or contamination of the intake TSG SST by ship heating. To remove these small offsets and examine only the variability due to a diurnal thermocline, the mean skin minus bulk temperature from 0:00 to 6:00 LMT was subtracted from the skin temperature. This two-step skin correction takes out the wind speed dependent cool skin effect using the modeled cool skin and then zeros the difference between skin-corrected SST_{skin} and SST_{depth}. The analysis reported here uses only days with clear signals of diurnal warming. These days were identified by examining both the M-AERI SST_{skin} and the TSG SST_{depth} to ensure that the apparent diurnal variability was not due to any extraneous bulk temperature changes such as caused by thermal fronts. Additionally, since days with clear signals of diurnal warming are typically on days with low winds and the diurnal thermocline is therefore shallow, it is unlikely that the TSG SST_{depth} has any significant diurnal warming that would contaminate our estimate of diurnal amplitudes. Furthermore, if the TSG SST_{depth} does have diurnal warming, it will result in an under-estimation of warming amplitudes. The magnitudes of diurnal warming in this study far exceed the small corrections for the cool skin effect and any secondary TSG offset.

4. Discussion

[24] In the following section, the general characteristics of diurnal warming using all 72 d of data will first be examined for dependencies on wind speed and insolation variability. Individual days that illustrate specific findings will be presented next. The examination of individual days shows directly how changes in wind speed or insolation affect the amplitude of the surface expression of diurnal warming. Finally, the temporal lag between changes in wind speed and insolation, and the changes in diurnal amplitudes will be determined from the available data.

[25] The largest warming event measured occurred at 13:12 LMT, 1.2 h after the maximum insolation. Figure 6 shows a histogram of the local time of the peak diurnal warming. While 18 d had a maximum warming at 12:00, the distribution is broad with a number of peak temperatures occurring later in the day. At 13:00, 14:00, and 15:00 LMT there were each 11 maximum warming events. The examination of all 72 d shows that the peak warming occurs at the time of the daily minimum wind speed, when sufficient heating is available (between 11:00 and 16:00). The shape of the peak does not echo the shape of the solar insolation forcing except on days with constant wind speed. Several days have two peaks and the shape of the temperature signal at the surface echoes the variability in wind speed.

[26] The measurements for all 72 d are shown in Figure 7 and reveal a maximum warming of 5.2 K. Figure 7 illustrates the diurnal variability as it depends on local time, wind speed, and insolation. In Figure 7a, diurnal warming is shown as a function of local time with each point colored by the wind speed at the time of the measurement. The warming is largest in the midafternoon at low wind speeds. From 6:00 to 8:00 LMT there is little to no diurnal warming, indicating that the M-AERI subskin temperature and the bulk temperatures are roughly equivalent. This early morning equivalence between the subskin and bulk temperatures supports the idea of a "foundation" temperature as defined in the Introduction. After sunrise, these temperatures often diverge because of diurnal warming. At wind speeds greater than 8 ms^{-1} there is negligible diurnal variability throughout the day. The surface of the ocean is still warmed by the sun, but with strong winds there is significant mixing and

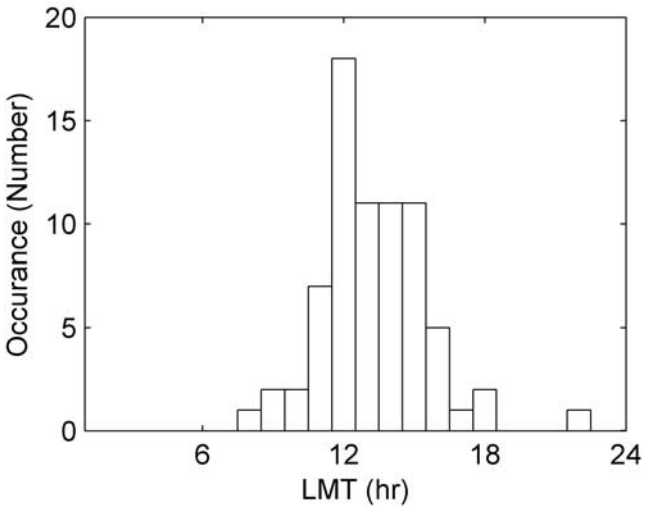

Figure 6. Histogram showing distribution of the daily maximum diurnal warming local mean time for the 72 d with diurnal warming.

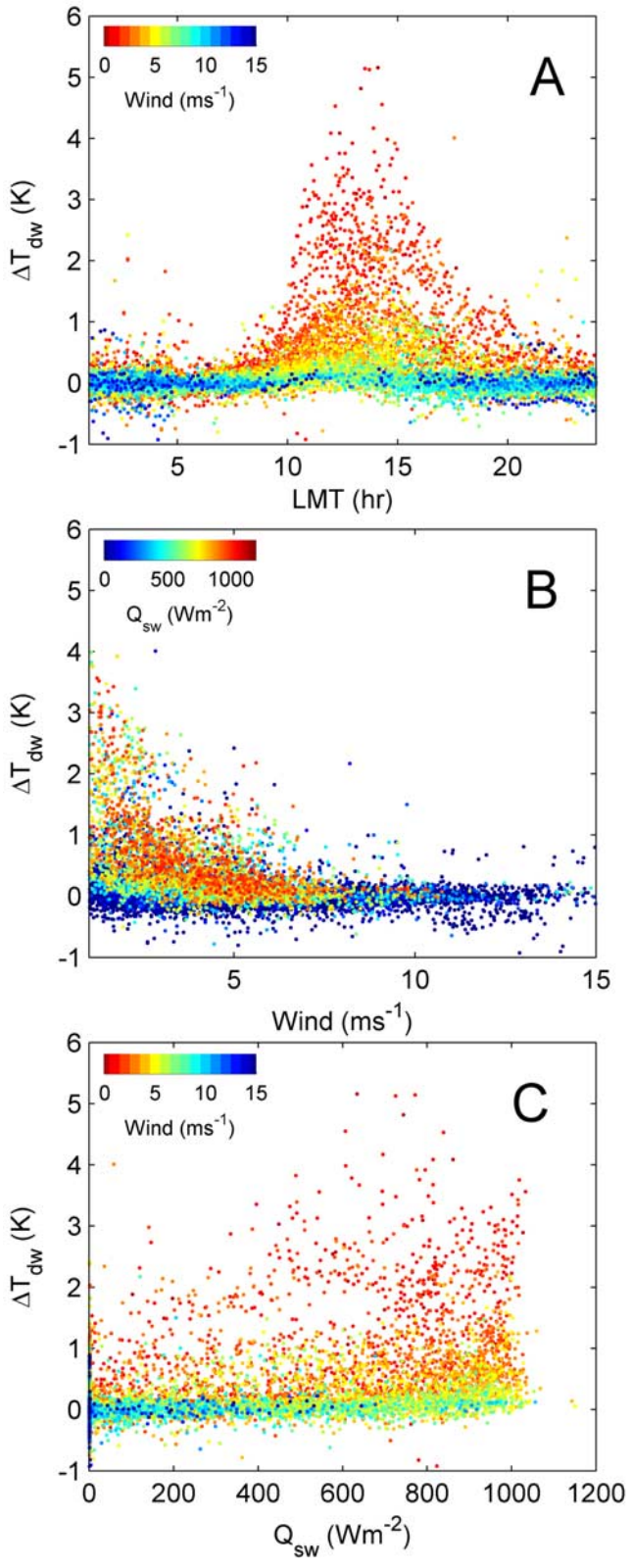

Figure 7. Diurnal warming as a function of (A) local time, (B) wind speed, and (C) shortwave insolation. ΔT_{dw} are shown for 72 d with clearly identified diurnal warming. Dot color definition is defined by the colorbar within each panel.

the warming is distributed over the entire mixed layer, resulting in little surface signature. Figure 7b shows the relationship between wind speed and diurnal warming, with insolation used for the color of dots. The largest warm events are at low wind speeds and high insolation. Figure 7c shows warming as a function of insolation, with wind speed indicated by the color of the dot. The largest warming events occur not at the maximum insolation, but slightly after it, at 600 to 800 Wm^{-2}. This lag is a result of both the lag in the occurrence of warming and insolation and also the sampled warming events. The largest warming events occurred at a minimum in wind speed that occurred after the peak in surface insolation.

[27] Measurements from several individual days are shown to illustrate the variability of diurnal warming (Figure 8 and Figure 9). Figure 8a shows the diurnal warming that occurred on 13 October 1999. This was the largest diurnal event measured, 5.2 K, at a wind speed of 0.5 ms^{-1} and insolation of 634 Wm^{-2} and at 13:12 LMT. At 14:06 LMT the wind began to increase, reached 5 ms^{-1}. The higher wind speeds quickly erased the diurnal warming measured at the surface. These data were taken from the R/V *Melville* on a day with very low winds and high insolation, the peak in warming occurred after the peak insolation. The solar insolation was measured on the ship and reached a maximum of 1106 Wm^{-2} at 12:00 LMT. There were no clouds during the entire day, so the insolation increased smoothly to its noon peak and then smoothly decreased.

[28] Another day (Figure 8b) with significant diurnal warming, from R/V *Ewing*, has a peak of 3.8 K that occurred at 12:36 LMT with a wind speed of 0.5 ms^{-1} and insolation of 1018 Wm^{-2}. The wind speed fluctuated during the day but was generally less than 3 ms^{-1}, with a minimum wind occurred at 7:44 LMT. These low winds resulted in increased warming, but the amplitude was small due to the low insolation. A second wind minimum occurred at 10:52 LMT and the diurnal warming increased to 3.6 K at 11:05 LMT, 13 min after the drop in wind speed. The next drop in wind speed occurred simultaneously with the largest diurnal peak at 12:36 LMT. The small increase in wind speed between 10:52 and 12:36 LMT caused the warming at the surface to decrease. This double peak in warming was a direct result of the two decreases in wind speed. After the second peak in warming, the wind speed increased to 3 ms^{-1} and the warming decreased slowly. The wind speed continued to stay below 4 ms^{-1} until late in the evening, resulting in little upper ocean mixing and the warming was still measurable at midnight.

[29] The previous two examples had large amplitudes of warming, with the peak during the middle of the day when insolation was large. The 72 d of warming revealed that the daily maximum temperature generally occurred soon after the daily minimum in wind speed rather than being controlled by the peak in insolation. Three more examples illustrate the close relationship between wind speed and diurnal warming. Maximum warming occurred in the morning on the 16 May 2003 (Figure 8c), afternoon of 9 Aug 2002 (Figure 8d), and late afternoon of 10 Nov 2001 (Figure 8e). On 16 May 2003, a minimum in wind speed occurred at 8:00 LMT and a maximum in warming slightly later, at 9:00 LMT. The wind speed increased and the warming decreased, disappearing completely by 13:00

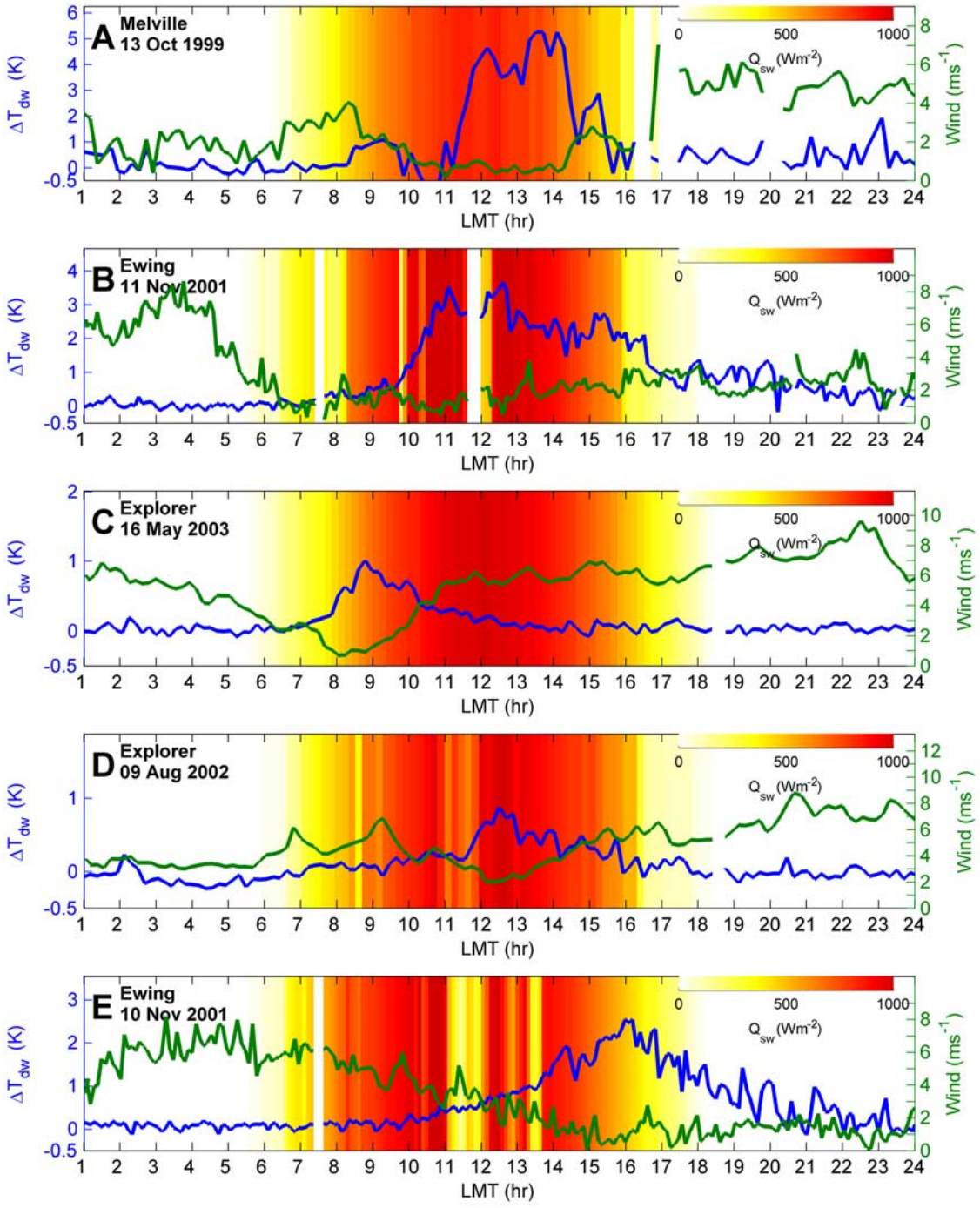

Figure 8. ΔT_{dw} (blue line) with scale is shown on the left axis, the wind speed (green line) with scale is on the right axis, the insolation is indicated by color in the background, and the cruise and date is indicated in the upper left corner.

LMT. On 9 Aug 2002 the minimum in wind speed occurred at 12:18 LMT, followed 11 min later by a maximum in warming. The wind speed then increased through the afternoon, rapidly erasing the surface expression of the warming. On 10 Nov 2001, the wind speed decreased through the day as the warming increased. A late afternoon minimum in wind speed occurred at 15:30 LMT and was followed, 30 min later, by a maximum in warming. After 15:30, the wind speeds remain low for the rest of the evening, allowing surface warming to be apparent late into the evening. The warming was finally erased by 21:00 LMT, long after sunset. This shows an example of the insolation having declined to zero, but the amplitude of warming was still significant as it takes some time for the surface heat fluxes and upper layer mixing to decrease the surface warming. These three figures illustrate the difficulty of simulating warming throughout the day without frequently measured wind and insolation. The heat available to the

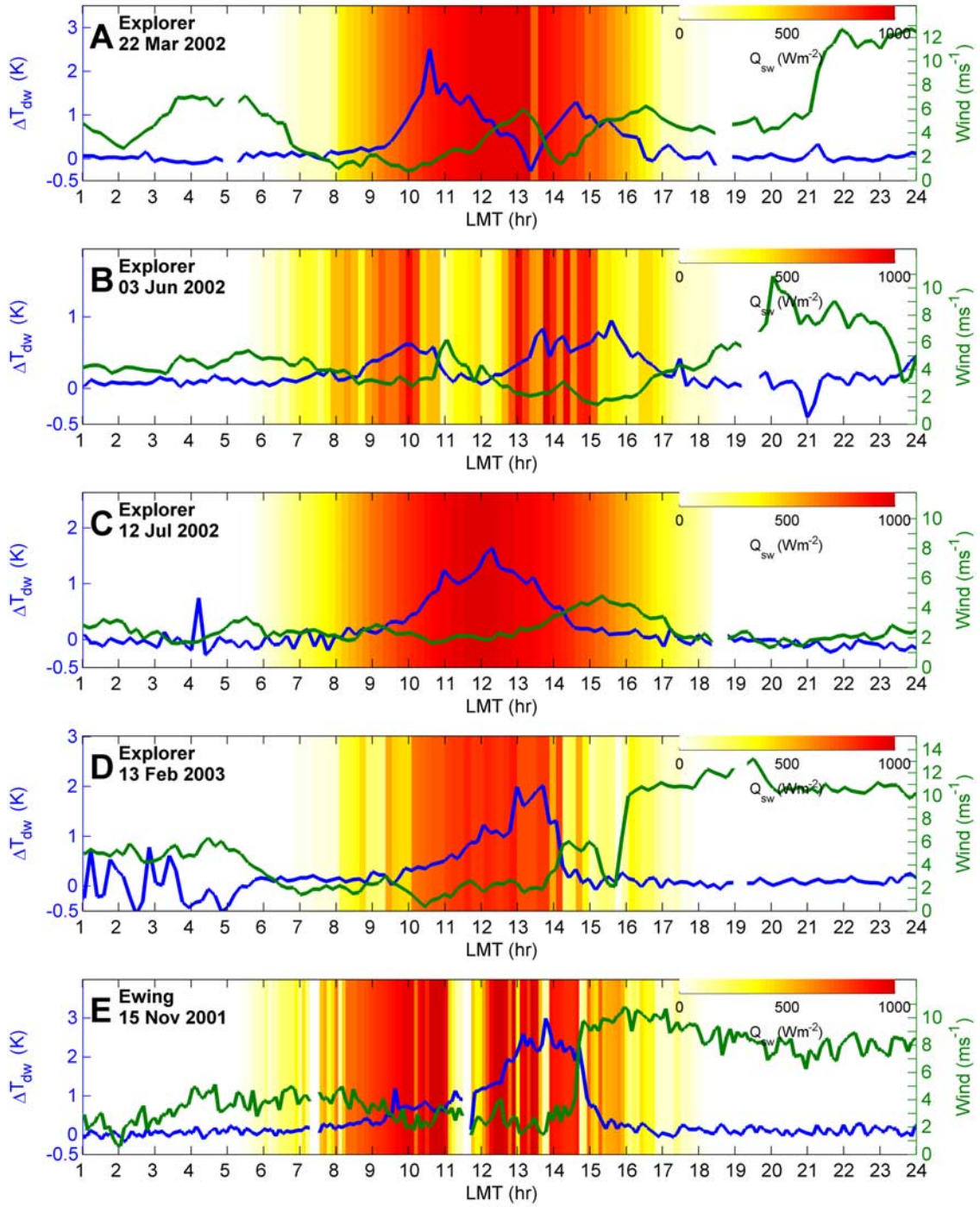

Figure 9. Examples of diurnal warming with formatting the same as described in Figure 8.

atmosphere can vary significantly due to the wind and insolation history.

[30] Figure 9a and Figure 9b again demonstrate how wind speed affected diurnal warming throughout the day. In these two cases, two drops in wind speed resulted in a double peak in diurnal warming. On 22 Mar 2002, the wind speed was less than 1 ms^{-1} and the surface rapidly warmed, increasing through 2.6 K at 10:36 LMT. The peak in warming occurred 39 min after the minimum in wind speed at 9:56 LMT. The decrease in warming after the 10:36 LMT peak was likely due to an increase in wind speed, since the insolation continually increased throughout this episode. The winds increased until 13:10 LMT and the diurnal warming decreased until 13:20 LMT. As winds decreased, after 13:10 LMT, there was a lag of 10 min before warming increased. A second diurnal peak occurred at 14:37 LMT, 25 min after the minimum in wind speed at 14:13 LMT. The diurnal warming was completely erased between the two peaks. Just after the minimum in warming between the two peaks, a cloud diminished the insolation, from 984 Wm^{-2} to 703 Wm^{-2}. It is difficult to infer any response in diurnal variability to this drop in insolation because the warming

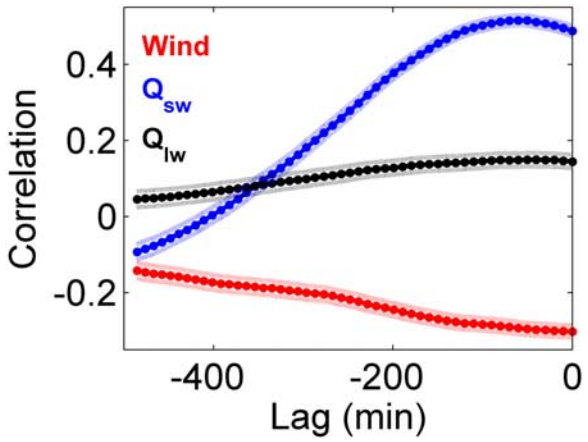

Figure 10. Lag correlation for M-AERI observed diurnal warming and measured wind speed, shortwave radiation, and downwelling longwave. The 95% confidence upper and lower bounds are shown with dotted lines.

was already erased by wind induced mixing. Another day, 3 June 2002, with two diurnal peaks is shown in Figure 9b. The larger peak was after the smaller peak. Similar to the previous example, the changes in diurnal warming lag changes in wind speed by 10 to 20 min. The first peak occurred at 9:55 LMT, with winds approximately 3 ms^{-1}. The second peak occurred at 15:35 LMT, but was preceded by several large fluctuations in diurnal warming that were not related to any obvious fluctuations in wind speed. Variations in insolation of approximately 350 Wm^{-2} were followed, 30 to 40 min later, by variations in diurnal warming. Wind-induced mixing erased surface warming rapidly, while, in the absence of wind mixing, changes in radiative forcing took almost twice as long to result in measurable changes.

[31] Figure 9c shows a clear-sky day with diurnal warming that follows a smooth bell shape. There were two small peaks in warming at 10:59 and 12:18 LMT. These small peaks were associated with small decreases in wind speed. The wind speed decreased to 1.7 ms^{-1} at 10:36 LMT followed, 23 min later by a local peak in warming. The wind speed decreased again, reaching a local minimum of 1.9 ms^{-1} at 12:07 LMT. The warming peaked 11 min later, at 12:18 LMT. The day was clear-sky with a maximum in insolation of 974 Wm^{-2} at 11:44 LMT. The wind speed increased in the afternoon and the warming decreased. When the wind reached 4.0 ms^{-1} the warming had diminished to less than 0.2 K. When the wind reached 4.4 ms^{-1} the warming diminished to less than 0.1 K.

[32] Diurnal warming with two equal peaks of 1.7 K at 13:00 and 13:40 LMT is shown in Figure 9d. The wind speed increased simultaneously with the decrease in diurnal warming. In the morning and late afternoon, fluctuations in the insolation were followed, approximately 40 min later, by changes in diurnal warming. The insolation changes of 100–200 Wm^{-2} were associated with changes in diurnal warming on the order of 0.1 to 0.2 K.

[33] An abrupt increase in wind speed, Figure 9e, at 14:40 caused a sharp decrease in warming at 14:50. Until 14:40, the wind speed was 3 to 5 ms^{-1}, within 20 min it increased to about 10 ms^{-1}. The insolation was variable, indicating that there was broken cloud cover. Between 11:00 and 12:00 the insolation decreased to approximately 100 Wm^{-2}, followed 30 min later by a decrease in diurnal warming.

[34] These individual days show that the warming responded rapidly to changes in wind speed and less rapidly or responsively to changes in insolation. To examine the temporal lag between changes in wind speed and insolation and the resulting response in the diurnal warming, the lag cross-correlations were calculated as:

$$r(\tau) = \frac{\Sigma(x_{i+\tau} - \langle x \rangle)(y_i - \langle y \rangle)}{(n-1)\sigma_x \sigma_y}, \tag{4}$$

where τ is the lag, x and y are the correlated variables, with the variables mean values indicated by $\langle\ \rangle$ and standard deviation by σ. The correlations for diurnal warming and wind speed, insolation, and downwelling longwave radiation are shown in Figure 10. The largest cross-correlation for diurnal warming and shortwave radiation is at a lag of 60 min, longwave radiation is at a lag of 50 min, and wind speed is 0 min. The measurements were mostly taken at roughly 10 min intervals which defines the increments in lag intervals. This indicates that changes in wind speed influenced diurnal amplitudes more rapidly than changes in radiative heating. The correlation for winds at zero lag are not statistically significantly different than winds with a 90 min lag at the 95% confidence interval.

[35] The temporal lag correlation between (1) insolation and diurnal warming and (2) wind speed and diurnal warming was calculated using daytime measurements from all 72 d with significant diurnal warming. Correlations with diurnal warming were positive for insolation and negative for wind speed, meaning that as insolation increases the surface warms, whereas increasing wind speed leads to diminished diurnal warming. The strongest correlations occurred for lags of 50 min for the insolation and 30 min for the wind speed. The lag-correlation for insolation is half its peak value in 2.5 h and not statistically significant after 3.3 h. The lag-correlation for wind speed is half its peak value in 3.6 h and not statistically significant after 6.6 h. These long tails may be partially due to the autocorrelation in the forcing fields.

[36] An important consideration when using cruise data is that the measurements are generally treated as a time series, giving the impression that the later measurements are related to earlier measurements at the same place. The ships used here were often moving and this is therefore only true when the spatial scales of diurnal warming events are larger than the distance covered by the ship. Since the diurnal warming is mainly controlled by wind speed and radiative fluxes, the spatial scales of these fields determines the spatial scales of diurnal warming. Spatial variability in winds is largest near land, but since most near-land data was removed from this study the variability in winds should be mostly due to large-scale weather patterns. The ship-based radiometer data are currently the best data available for studies of diurnal warming. Ideally, data for diurnal warming would be taken at a single location so as to observe the complete radiative and momentum fluxes. This may not be possible from a research vessel, as when the ship is stationary it quickly disturbs the surrounding waters

contaminating the data. A skin temperature radiometer mounted on a small platform or buoy would provide a solution, but currently, this is not feasible.

5. Conclusions

[37] The M-AERI data and ancillary meteorological and oceanographic measurements used here were collected on five cruises, spanning all major ocean basins from the Tropics to the Southern Ocean. The maximum warming observed was 5.2 K in the Gulf of California on a very calm, very sunny day. There were nine measurements of warming over 4.0 K in the entire data set, all from the R/V *Melville* cruise. While the R/V *Melville* cruise occurred in a relatively protected environment, large diurnal events have been found to exist elsewhere [*Yokoyama et al.*, 1995].

[38] Examination of the 72 d with significant warming showed extremely variable diurnal signatures. Given sufficient solar forcing, the daily peak or peaks occurred at wind speed minima. Peaks in warming occur between 8:00 and 18:00 LMT, with the majority occurring at 12:00 (18 occurrences), and many peaks (33 events) also occurring between 13:00 and 16:00 LMT. The histogram of peak warming, initially support the idea of a simple warming models that only estimate the peak warming value, such as *Kawai and Kawamura* [2002] or *Webster et al.* [1996], but the large numbers of peaks away from the solar peak emphasize the necessity of resolving intraday variability for accurate calculation of diurnal heating.

[39] These results show that the surface signature of diurnal warming is primarily related to wind speed and secondarily to insolation. Relatively small changes in wind speed rapidly and strongly affect the amplitude of diurnal warming present in the sea surface. The daily peak in diurnal warming is directly related to the minimum wind speed during the day, causing the time of the peak to shift depending on when the minimum winds occur. Fluctuations in wind speed can result in multiple peaks in diurnal heating. When the wind speed rapidly increases to above 6 ms^{-1}, warming can be completely erased from the SST_{skin} measurement in as quickly as 30 min. For all the days with diurnal warming the strongest lag-correlation between wind speed and diurnal warming occurred at 30 min (i.e., two to three measurement cycles of the M-AERI measurements used here). Fluctuations in insolation need to be large (over 100 Wm^{-2}) to cause a measurable effect (0.1 to 0.2 K) on the diurnal signal and the strongest correlation is at a 50 min lag. These results imply that near-simultaneous wind and insolation measurements are important for accurately modeling diurnal warming. Future work will include comparing these data to several of the diurnal warming models, including some that have been specifically simplified for global, near-real-time application to satellite SST measurements.

Appendix A

A1. *Explorer of the Seas*

[40] With any autonomous instrument, a number of things may go wrong and not be flagged within the automated data stream. In four years of data, there were only a few days that needed to be excluded because of questionable measurements. For example, on 3–4 April 2001, the bulk temperature warmed considerably, which were subsequently determined to result from the shutting off the bow thruster ship intake pump. Since mid-2002, intake flow rate was available and the bulk SST was flagged when flow rates fall below 15 $Lmin^{-1}$. For earlier data, bulk SST data were visually identified and excluded from further analysis. When stationary, the heat of the ship rapidly affected measurements, resulting in a warming in the SST measurements. Therefore when the ship speed was below 10 kts (calculated from the navigation data), measurements were excluded from the data set.

[41] Comparing the bulk and M-AERI skin temperatures is a useful initial check on the accuracy of the measurements. On 29 November 2002 and 26 January 2003 either the skin or bulk temperatures appear to have instrumental problems. Since we are unable to determine which is actually in error, both are excluded from the data set. On 3 July 2003 the M-AERI temperature is 1.5 K warmer than the intake temperature for approximately 24 h. It does not look like a real excursion and this day has been removed from the data set. From 9–11 May 2004 the M-AERI retrieval has much more variability than normal and these data were excluded from further analysis. The source of these errors is not known. M-AERI and bulk TSG SST data may become influenced by shallow water and land effects when the ship is within 20 km of land and these data were excluded from further analysis.

[42] The apparent wind direction is the direction measured by the wind vane relative to true North, using the meteorological standard where the direction given is the direction from which the wind is blowing. The apparent wind speed is the sum of the relative wind direction, the ship's heading, and the zero-line reference angle. To calculate the true wind speed and direction, one must correct for the ship's speed and heading. The "true" wind should also be corrected for the wind field distortion due to the ship's size and relative heading to the wind field but it is unclear, without extensive wind modeling studies, how to proceed with this correction [*Popinet et al.*, 2004]. Both the apparent and "true" winds were included in the analysis to help in determining the "best" wind.

A2. R/V *Aurora Australis*

[43] According to ship documentation, "when the apparent wind direction is approximately 190° to 240°, readings from the starboard anemometer can be more scattered and higher compared to port" and "When apparent wind direction is around 135°, wind speed readings from the port sensor decrease relative to the starboard sensor and are marked bad. Similarly, when apparent wind direction is about 225°, starboard readings are lower than port and therefore rejected" (http://aadc-maps.aad.gov.au/metadata/mar_sci/Dz200203020.html). Apparent wind direction of 120° to 170°, can affect the port sensor readings in the same way. This reported problem was confirmed in this study. The reported "true" wind speed and direction were examined for ship effects. The difference (port–starboard) between the reported true wind directions and wind speeds as a function of measured apparent port wind direction was examined for wind shadowing. It was found that for certain wind directions the wind speed on either the port or starboard side is shadowed. When the wind direction is

from the aft and cross ship, the upwind anemometer measures a higher wind speed than the downwind anemometer when the ship superstructure is blocking the downwind anemometer. Apparent wind directions from the forward or aft directions are generally similar for both anemometers. These results were used to select the upwind anemometer.

[44] Port and starboard measurements were averaged to a single value for air temperature, humidity, and solar radiation. The nearest 1-min meteorological data were combined with the M-AERI measurements. Data were examined visually for problems. It was determined that the port anemometer showed very low wind speeds at approximately day 29 September through 2 October. These were furthered examined and it was found that although the winds were not flagged as bad data, the apparent wind direction was approximately 265° and the wind speeds were low for this period, indicating of some type of instrument malfunction. The port wind measurements for these days were flagged and removed from the data set.

A3. R/V *Ewing*

[45] During the cruise, raw data were visually examined for outliers and interruptions in data acquisition. For this cruise, the M-AERI retrieved air temperature and skin temperature approximately every 6 min. The meteorological data are a best compilation of data derived from a portable weather station and the ship's meteorological measurements. All reported values were averaged into 1-min values, and the reported wind speed was corrected to a 10 m height. The nearest 1-min meteorological data were matched with the M-AERI measurements. Data were visually examined for problems and several bad values for TSG temperatures were removed from further analysis.

A4. R/V *Melville*

[46] Data were visually examined for outliers. The outliers were removed and all relevant variables were collocated with the M-AERI data.

A5. R/V *Revelle*

[47] There were significantly more questionable measurements during this cruise. A number of methods for editing the questionable M-AERI retrievals were examined. Data from 5 October 9:00 LMT to 6 October 7:00 LMT and the entire day 11 October were removed because of large errors. Large differences (less than −1.0 K or greater than 2.5 K) in the skin minus air temperatures or (less than −0.5 K or greater than 2.0 K) skin minus bulk TSG temperature were removed. After erroneous data were removed, all relevant variables were resampled to the closest M-AERI data.

[48] **Acknowledgments.** We would like to acknowledge the contributions of Nick Shay, Ian Robinson, Bob Evans, and Eric Chassignet. The data for this study were collected by Eddie Kearns and Bob Evans (R/V *Melville*), Chip Maxwell and Don Cucchiara (*Explorer of the Seas*), and Erica Key (R/V *Ewing* and R/V Aurora). This work was supported by funding from NOAA (NA030AR4310126) and NASA (NM0710772, NAG5-11104, NNG04HZ33C, and NAS5-31361).

References

Chen, S. S., and R. A. Houze (1997), Diurnal variation and lifecycle of deep convective systems over the tropical Pacific warm pool, *Q. J. R. Meteorol. Soc.*, *123*, 357–388.

Defant, A. (1961), *Physical Oceanography*, Elsevier, New York.

Delnore, V. E. (1972), Diurnal variation of temperature and energy budget for the oceanic mixed layer during BOMEX, *J. Phys. Oceanogr.*, *2*, 239–247.

Deschamps, P. Y., and R. Frouin (1984), Large diurnal heating of the sea surface observed by the HCMR Experiment, *J. Phys. Oceanogr.*, *14*, 177–185.

Donlon, C. J., P. J. Minnett, I. J. Barton, T. J. Nightingale, and C. L. Gentemann (2001), *The Character of Skin and Subsurface Sea Surface Temperature*, World Meteorol. Organ., Geneva, Switzerland.

Donlon, C. J., P. J. Minnett, C. L. Gentemann, I. J. Barton, B. Ward, J. Murray, and T. J. Nightingale (2002), Towards improved validation of satellite sea surface skin temperature measurements for climate research, *J. Clim.*, *15*(4), 353–369.

Donlon, C. J., et al. (2007), The Global Ocean Data Assimilation Experiment (GODAE) High Resolution Sea Surface Temperature Pilot Project (GHRSST-PP), *Bull. Am. Meteorol. Soc.*, *88*(8), 1197–1213.

Fairall, C. W., E. F. Bradley, J. S. Godfrey, G. A. Wick, J. B. Edson, and G. S. Young (1996), Cool-skin and warm-layer effects on sea surface temperature, *J. Geophys. Res.*, *101*(C1), 1295–1308.

Flament, P., M. Firing, M. Sawyer, and C. Trefois (1994), Amplitude and horizontal structure of a large diurnal sea surface arming event during the coastal ocean dynamics experiment, *J. Phys. Oceanogr.*, *24*(1), 124–139.

Gentemann, C. L. (2007), Diurnal warming at the ocean surface, Ph.D. thesis, 163 pp., Univ. of Miami, Meteorol. and Phys. Oceanogr., Miami, Fla.

Gentemann, C. L., C. J. Donlon, A. Stuart-Menteth, and F. J. Wentz (2003), Diurnal signals in satellite sea surface temperature measurements, *Geophys. Res. Lett.*, *30*(3), 1140, doi:10.1029/2002GL016291.

GOOS Implementation Advisory Group (IAG) (1999), *Global Physical Ocean Observations for GOOS/GCOS - An Action Plan for Existing Bodies and Mechanisms*, UNESCO, Paris, France.

Halpern, D., and R. Reed (1976), Heat budget of the upper ocean under light winds, *J. Phys. Oceanogr.*, *6*, 972–976.

Horrocks, L. A., B. Candy, T. J. Nightingale, R. W. Saunders, A. G. O'Carroll, and A. R. Harris (2003), Parameterizations of the ocean skin effect and implications for satellite-based measurement of sea-surface temperature, *J. Geophys. Res.*, *108*(C3), 3069, doi:10.1029/2002JC001503.

Hosom, D. S., R. A. Weller, R. E. Payne, and K. E. Prada (1995), The IMET (Improved Meteorology) ship and buoy system, *J. Atmos. Oceanic Technol.*, *12*(3), 527–540.

Jessup, A., and R. Branch (2008), Integrated ocean skin and bulk temperature using the calibrated infrared in situ measurement system (CIRIMS) and through-hull ports, *J. Atmos. Oceanic Technol.*, *25*(4), 579–597, doi:10.1175/2007JTECHO479.1.

Kaiser, J. A. (1978), Heat balance of the upper ocean under light winds, *J. Phys. Oceanogr.*, *8*, 1–12.

Kawai, Y., and H. Kawamura (2002), Evaluation of the diurnal warming of sea surface temperatures using satellite-derived marine meteorological data, *J. Oceanogr.*, *58*(6), 805–814.

Kawai, Y., and A. Wada (2007), Diurnal sea surface temperature variation and its impact on the atmosphere and ocean: A review, *J. Oceanogr.*, *63*(5), 721–877.

Knuteson, R. O., et al. (2004a), Atmospheric Emitted Radiance Interferometer. part I: Instrument Design, *J. Atmos. Oceanic Technol.*, *21*(12), 1763–1776.

Knuteson, R. O., et al. (2004b), Atmospheric Emitted Radiance Interferometer. part II: Instrument Performance, *J. Atmos. Oceanic Technol.*, *21*(12), 1777–1789.

Kummerow, C., W. Barnes, T. Kozu, J. Shieu, and J. Simpson (1998), The tropical rainfall measuring mission (TRMM) sensor package, *J. Atmos. Oceanic Technol.*, *15*(3), 809–817.

Mears, C. A., D. K. Smith, and F. J. Wentz (2001), Comparison of Special Sensor Microwave Imager and buoy-measured wind speeds from 1987–1997, *J. Geophys. Res.*, *106*(C6), 11,719–11,729.

Merchant, C. J., M. J. Filipiak, P. Le Borgne, H. Roquet, E. Autret, J.-F. Piollé, and S. Lavender (2008), Diurnal warm-layer events in the western Mediterranean and European shelf seas, *Geophys. Res. Lett.*, *35*, L04601, doi:10.1029/2007GL033071.

Minnett, P. J. (2003), Radiometric measurements of the sea-surface skin temperature-the competing roles of the diurnal thermocline and the cool skin, *Int. J. Remote Sens.*, *24*(24), 5033–5047.

Minnett, P. J., and B. Ward (2000), Measurements of near-surface ocean temperature variability–consequences on the validation of AATSR on Envisat, in Proceedings of the ERS–ENVISAT Symposium "Looking down to Earth in the New Millennium", *Eur. Space Agency Spec. Publ.*, *ESA-SP*, Gothenburg, Sweden.

Minnett, P. J., R. O. Knuteson, F. A. Best, B. J. Osborne, J. A. Hanafin, and O. B. Brown (2001), The Marine-Atmospheric Emitted Radiance Interferometer (M-AERI), a high-accuracy, sea-going infrared spectroradiometer, *J. Atmos. Oceanic Technol.*, *18*, 994–1013.

Palmer, T. N., and D. A. Mansfield (1984), Response of two atmospheric general circulation models to sea-surface temperature anomalies in the tropical East and West Pacific, *Nature*, *310*(5977), 483–485.

Popinet, S., M. Smith, and C. Stevens (2004), Experimental and numerical study of the turbulence characteristics of airflow around a research vessel, *J. Atmos. Oceanic Technol.*, *21*, 1575–1590.

Rice, J. P., S. C. Bender, W. H. Atkins, and F. J. Lovas (2003), Deployment test of the NIST EOS thermal-infrared transfer radiometer, *Int. J. Remote Sens.*, *24*(2), 367–388.

Schluessel, P., W. J. Emery, H. Grassl, and T. Mammen (1990), On the bulk-skin temperature difference and its impact on satellite remote sensing of sea surface temperature, *J. Geophys. Res.*, *95*(C8), 13,341–13,356.

Shukla, J. (1998), Predictability in the midst of chaos: A scientific basis for climate forecasting, *Science*, *282*(5389), 728–731.

Stommel, H. (1969), Observations of the diurnal thermocline, *Deep Sea Res., Part I*, *16*, 269–284.

Stommel, H., and A. H. Woodcock (1951), Diurnal heating of the surface of the Gulf of Mexico in the spring of 1942, *Eos Trans. AGU*, *32*(4), 565–571.

Stramma, L., P. Cornillon, R. A. Weller, J. F. Price, and M. G. Briscoe (1986), Large diurnal sea surface temperature variability: Satellite and in situ measurements, *J. Phys. Oceanogr.*, *16*, 827–837.

Sverdrup, H. U., M. W. Johnson, and R. H. Fleming (1942), *The Oceans: Their Physics, Chemistry, and General Biology*, Prentice-Hall, Englewood Cliff, N. J.

Ward, B. (2006), Near-surface ocean temperature, *J. Geophys. Res.*, *111*, C02005, doi:10.1029/2004JC002689.

Webster, P. J., C. A. Clayson, and J. A. Curry (1996), Clouds, radiation, and the diurnal cycle of sea surface temperature in the tropical western Pacific, *J. Clim.*, *9*, 1712–1730.

Wentz, F. J. (1997), A well calibrated ocean algorithm for special sensor microwave/imager, *J. Geophys. Res.*, *102*(C4), 8703–8718.

Wentz, F. J., C. L. Gentemann, D. K. Smith, and D. B. Chelton (2000), Satellite measurements of sea surface temperature through clouds, *Science*, *288*(5467), 847–850.

Williams, E. J., R. G. Zika, O. B. Brown, and P. B. Ortner (2006), Utilization of a commercial cruise liner as a Voluntary Observing Ship (VOS) and research platform, paper presented at the 13th Ocean Sciences Meeting, AGU, Honolulu, Hawaii, 20-24 Feb.

Woods, J. D., and W. Barkmann (1986), The response of the upper ocean to solar heating. Part I: The mixed layer, *Q. J. R. Meteorol. Soc.*, *112*, 1–27.

Woods, J. D., W. Barkmann, and A. Horch (1984), Solar heating of the oceans-diurnal, seasonal, and meridional variations, *Q. J. R. Meteorol. Soc.*, *110*, 633–686.

Yokoyama, R., S. Tanba, and T. Souma (1995), Sea surface effects on the sea surface temperature estimation by remote sensing, *Int. J. Remote Sens.*, *16*, 227–238.

C. L. Gentemann, Remote Sensing Systems, 438 First Street, Suite 200, Santa Rosa, CA 95401, USA. (gentemann@remss.com)

P. J. Minnett, Rosenstiel School of Marine and Atmospheric Science, University of Miami, 4600 Rickenbacker Causeway, Miami, FL 33149, USA. (pminnett@rsmas.miami.edu)